Poly(aryl piperidium)-based AEMs utilizing spirobifluorene as a branching agent

Geun Woong Ryoo,[1,†] Sang Hun Shin,[2,†] In Wook Song,[1] Ki Chang Kwon,[3] Sun Hwa Park,[3,*] Jang Yong Lee,[2,*] Min Sang Kwon[1,*]

[1]Department of Materials Science and Engineering, Research Institute of Advanced Materials, Seoul National University, Seoul, Republic of Korea

[2]Energy Materials Research Center, Korea Research Institute of Chemical Technology (KRICT), Daejeon 34114, Republic of Korea.

[3]Interdisciplinary Materials Measurement Institute, Korea Research Institute of Standards and Science (KRISS), Daejeon 34113, Republic of Korea

*Corresponding author: psh@kriss.re.kr; ljylee@krict.re.kr; minsang@snu.ac.kr

[†]These authors contributed equally: G.W. Ryoo and S.H. Shin

ABSTRACT

We here developed high-performance anion exchange membranes (AEMs) by incorporating 9,9'-spirobifluorene as a three-dimensional branching agent, addressing the common trade-off between ion conductivity and dimensional/mechanical stability. By fine-tuning the ratio of terphenyl to biphenyl and the amount of the branching agent, we refined the AEM, achieving high conductivity (approximately 190 mS/cm at 80 °C in 1 M KOH) with decent dimensional/mechanical properties, comparable to the recently reported state-of-the-art membranes. Investigations using gas pycnometry and atomic force microscopy demonstrated that spirobifluorene enhances the fractional free volume around the membrane's backbone and more precisely modulates the separation between hydrophobic and hydrophilic domains, thus boosting both ion conductivity and mechanical stability. This membrane also displayed excellent chemical stability, with negligible degradation at 80 °C in 1 M KOH over 1000 h. With such a membrane, we achieved excellent cell performance, with a current density of 11.2 A/cm² at 80 °C, 2 V.

INTRODUCTION

To achieve carbon neutrality in the coming decades, hydrogen technologies like fuel cells and water electrolysis systems are critical.[1] Among hydrogen production methods, integrating ion exchange membrane water electrolysis with renewable energy sources, such as solar power, is a leading approach.[2] However, the commonly used proton exchange membrane water electrolyzers (PEMWEs) are hampered by their dependence on expensive platinum group metals (PGMs).[3] A promising solution to this challenge is the development of anion exchange membrane water electrolyzers (AEMWEs).[4] This alternative not only avoids the need for PGM catalysts but also offers faster oxygen evolution kinetics.

The development of AEMWEs has been hindered by the lack of suitable AEMs and ionomers that meet essential commercialization criteria, including hydroxide ion conductivity, resistance to alkaline conditions, and dimensional and mechanical stability.[5] Identifying materials that maintain chemical stability in alkaline environments has become a primary challenge in the field.[6] In response, extensive research has been conducted to understand the causes of polymer degradation under these conditions.[4, 7] This research has led to the creation of innovative polymer structures, especially those without arylether linkages,[8] and the introduction of durable organic cations,[4, 9] markedly improving chemical stability.[10] However, despite these advancements, further developments are essential for commercialization.[11]

Another important issue is balancing ion conductivity with dimensional and mechanical stability, as these attributes are typically in a trade-off relationship.[12] Enhanced ion conductivity generally requires an increase in the quantity of organic cations, thus raising the ion exchange capacity (IEC).[13] However, a higher IEC leads to increased water uptake (WU) by the polymer, resulting in a higher swelling ratio (SR), which can compromise the polymer's structural integrity.[14] To address this issue, various strategies have been introduced, including morphological engineering using block or side-chain techniques.[15] In a notable example, Xu, Yan, and coworkers integrated 2,2,2-trifluoroacetophenone—a hydrophobic building block of considerable reactivity—into the structure of poly(aryl piperidinium) (PAP-TP-85; Strategy I, see ***Figure 1a***).[16] This modification aimed to significantly increase the molecular weight of the polymer, thereby augmenting its inherent hydrophobic properties. As a result, such a strategic approach effectively mitigated the prevailing trade-offs. A more successful approach has recently emerged, involving the introduction of branching within the polymer backbone through multi-armed aromatic building blocks.[17] This simultaneously enhances ion conductivity and mechanical/dimensional stability. Lee, Hu, and colleagues have showcased the use of triphenylbenzene as a branching agent in poly(p-terphenyl piperidinium), achieving improved dimensional stability and conductivity over its linear counterparts (b-PTP-2.5; Strategy II, see ***Figure 1a***).[18] Similarly, Li and co-researchers have applied the same branching agent in poly(arylene alkylene)s, resulting in a marked increase in conductivity and a significant decrease in SR.[19] Most recently, Lee's team utilized triptycene, a

three-dimensional (3D) branching agent, achieving an impressive ion conductivity of 193.5 mS/cm with a moderate SR near 20% (b-PDTP-Trip-5; Strategy III, see ***Figure 1a***).[20] Interestingly, as the concentration of triptycene increases, the SR decreases while WU increases, suggesting a significant free volume among the polymer chains. This indicates that such a vast free volume is crucial for the observed increase in ion conductivity.

In this study, we introduce a new 3D branching agent, i.e. spirobifluorene, which significantly enhances ion conductivity, mechanical toughness, and SR simultaneously (***Figure 1b***). Compared to triptycene, spirobifluorene functions as a 4-arm crosslinker with a tetrahedral structure, exhibiting similar properties at a lower molar incorporation of approximately 2%. Additionally, by adjusting the ratio of terphenyl to biphenyl and the concentration of the branching agent within the poly(aryl piperidinium) backbone, we optimized both ion conductivity and SR. Notably, increasing the biphenyl content while also raising the concentration of the branching agent led to a consistent SR along with a sharp increase in ion conductivity.[21] This trend indicates that the enhanced ion conductivity, driven by an increased IEC due to the higher biphenyl content, is balanced by improved crosslinking from the increased concentration of the branching agent. Moreover, when spirobifluorene was introduced as a branching agent, it was observed to provide low SR and enhance ionic conductivity by offering additional free volume. These results support the effectiveness of the 3D branching agent strategy in simultaneously enhancing ion conductivity and dimensional stability. Furthermore, excellent cell performance corresponding to 11.2 A/cm^2 at 80 ºC, 2 V was achieved. We believe that systematically optimizing physical properties through control over the backbone structure and branching agent composition will pave the way for the development of high-performance AEMs in the future.

RESULTS AND DISCUSSION

Design and synthesis of AEMs

Poly(aryl piperidinium) is renowned for its decent chemical stability and its ease of synthesis, which allows for straightforward customization.[22] The structural diversity enables precise control over physical properties, making it the backbone framework of choice in the study of AEMs and ionomers.[23] Given these advantages, we chose poly(aryl piperidinium) as the backbone and spirobifluorene as the branching agent. As previously discussed, we aimed to optimize ion conductivity, SR, and WU by fine-tuning the ratios of biphenyl to terphenyl and the proportion of branching agent.

We synthesized six distinct branched polymers through a super-acid catalyzed reaction, each characterized by a unique ratio of biphenyl to terphenyl and varying amounts of the branching agent (***Figure***

1b and Figures S2-4). The polymers include: i) Terphenyl-based polymers, each containing 1 mol% (PTPIPQ-SF1) and 2 mol% (PTPIPQ-SF2) spirobifluorene; ii) Biphenyl-based polymers, enriched with 1 mol% (PBPIPQ-SF1) and 2 mol% (PBPIPQ-SF2) spirobifluorene; iii) Polymers formulated with a biphenyl to terphenyl molar ratio of 2:8, and infused with either 1 mol% (PBTPIPQ-SF1) or 2 mol% (PBTPIPQ-SF2) spirobifluorene. As illustrated in ***Figure S2***, the chemical structures of these polymers were verified via ^{1}H NMR spectra. The peaks at 6.52, 7.09, 7.36 and 7.99 ppm are associated with the protons from spirobifluorene, respectively, which suggests their successful synthesis. Through NMR comparison before and after quaternization, we determined that quaternization did not alter the polymer structure, as evidenced by the ^{1}H NMR spectrum of the polymers (***Figures S5-7***). Also, Mohr titration revealed that the ion exchange capacities (IECs) of all the synthesized polymers were similar to their theoretical values, demonstrating complete conversion in the quaternization reactions (***Table 1***).

We then prepared membranes with an approximate thickness of 40 μm using the prepared polymers. The membranes incorporated iodide as the counter anion. Initially, a 10 wt% polymer solution in dimethyl sulfoxide (DMSO) was prepared. This solution was spread on a glass plate using a doctor blade, and the solvent was subsequently evaporated on a hot plate to form a film. Of the six polymers prepared, five—PBPIPQ-SF1/2, PTPIPQ-SF1, PBTPIPQ-SF1 /2—consistently produced uniformly well-formed membranes. However, the creation of the film with PTPIPQ-SF2 was hampered by gelation, a direct consequence of its diminished solubility. Additionally, PBPIPQ-SF1 formed a film effectively, but excessive swelling was observed. This is believed to be due to the increased IEC resulting from the high biphenyl content and the decreased crosslinking density from the low spirobifluorene content. Notably, this phenomenon was not observed when the terphenyl content and/or the spirofluorene content was increased (in PTPIPQ-SF1 and PBTPIPQ-SF1/2, respectively). As is well known, excessive swelling significantly compromises mechanical and dimensional stability, thereby reducing long-term usability and making the polymers unsuitable for use as membranes.[24] Consequently, subsequent experiments involved three types of polymers that demonstrated sufficient solubility, good film processability, and no excessive swelling (***Table 1***). For comparative analysis, we used PAP-TP-85, also known as PiperION, which we synthesized ourselves, and FAA-3, a product by Fumatech, which we purchased.

Properties of AEMs

We first measured the SR, WU, and ion conductivity for PAP-TP-85 and FAA-3, with detailed measurement methods described in the supporting information (SI).[25] Although the measured data showed some differences compared to previously reported data, they matched well overall, confirming the reliability of our experiments.

Figures 2a-c display the WU, SR, and ion conductivities of the prepared membranes over a temperature range from 30 to 80 °C; the specific values are listed in ***Table 1***. Spirobifluorene-branched PTPIPQ-SF1 exhibits a decent ionic conductivity of 155 mS/cm at 80 °C, which is better than the 138 mS/cm reported for PTPIPQ without a branching agent.[26] While PTPIPQ-SF1 exhibited improved conductivity, both WU and SR were reduced as compared to PTPIPQ, aligning with trends observed in studies using 3D branching agents.[18-19, 27]. PBPIPQ-SF1, designed to increase IEC by maintaining spirobifluorene at 1 mol% and substituting terphenyl with biphenyl, demonstrated significantly increased conductivity of 190 mS/cm. However, it also showed excessive WU (> 900%) and SR (> 100%). PBTPIPQ-SF1, an AEM where spirobifluorene was kept at 1 mol% and 20 mol% of terphenyl was replaced with biphenyl, exhibited a more balanced profile in terms of ionic conductivity, WU, and SR. Compared to PBPIPQ-SF1, its conductivity was slightly lower at 175 mS/cm, but it displayed much better dimensional stability. Optimal properties were observed in PBTPIPQ-SF2, where the spirofluorene content was increased by 1 mol% from PBTPIPQ-SF1. Although WU and SR slightly decreased, conductivity rose to 190 mS/cm, nearly matching that of PBPIPQ-SF1; as shown in ***Figure 2d***, the ion conductivity and dimensional stability observed in PBTPIPQ-SF2 are values close to the state-of-the-art. These results are counterintuitive to the general understanding that conductivity and the WU/SR typically have a trade-off relationship. This implies that, as proposed by others, the use of spirobifluorene as a 3D branching agent may facilitate the formation of interconnected channels and/or provide a significant amount of free volume near the backbone where ions to be conducted.[18-19, 27] In fact, it is known that in AEMs, OH^- conduction is facilitated by both the vehicular mechanism and the Grotthuss mechanism, with an appropriate amount of free volume near the backbone being crucial.[28]

Morphology

To elucidate this behavior, we employed a gas pycnometer to measure the fractional free volume (FFV), correlated with the difference between the skeletal volume (V_0) and the apparent volume (V) (***Equations 1-3***).[29] V represents the specific apparent volume of the AEM, V_0 is the specific skeletal volume of the polymer, and V_{dry} is the volume of dry membrane measured by gas pycnometer. To ensure precise measurements, the apparent volume was determined by cutting the membrane into 1 x 1 cm^2 and subsequently measuring their respective thickness.

$$FFV = (V - V_0)/V \quad (1)$$

$$V = \sum_{i=1}^{50}(1 \times 1 \times t_i) \ / m_{dry} \quad (2)$$

$$V_0 = V_{dry} / m_{dry} \quad (3)$$

As depicted in ***Figure 3a***, a comparison between PBTPIPQ-SF1 and SF2 shows that as the amount of the

branching agent increased, so did the FFV, correlating with the trend in conductivity. These results suggest that the tetrahedral structure of spirobifluorene allows for more free volume around the backbone, thereby increasing conductivity.[30] When the same amount of branching agent was used, the FFV tended to increase with the amount of terphenyl (comparing PTPIPQ-SF1 with PBTPIPQ-SF1). Despite having a higher FFV, PTPIPQ-SF1 exhibited lower conductivity compared to PBTPIPQ-SF1 (155 vs 175 mS/cm at 80 °C), which is likely due to the slightly higher IEC (2.68 vs 2.87 mmol/g) and WU (76.7 vs 96.6% at 80 °C) of PBTPIPQ-SF1.

The incorporation of 3D branching agents with large free volumes has been known to increase microphase separation and lead to the formation of more interconnected channels.[20, 27, 31] The interconnected channels, induced by aggregation of hydrophilic domains, are believed to facilitate ion transport via the vehicular and Grotthuss mechanisms, thereby enhancing ionic conductivity[31a, 32] A related previous study that employed triptycene and tetraphenylmethane as 3D branching agents suggested the formation of interconnected channels.[20, 27] This was corroborated by evidence of microphase separation observed in surface topology studies conducted with AFM. As depicted in ***Figure 3b***, and consistent with previous studies, PBTPIPQ-SF2 displayed markedly clearer bright and dark regions than PTPIPQ-SF1 and PBTPIPQ-SF1. This enhanced clarity in the AFM images indicates improved microphase separation, which suggests a beneficial effect from increased spirobifluorene incorporation. Additionally, when comparing PBTPIPQ-SF1 and PBTPIPQ-SF2, the latter shows a more continuous arrangement of aggregated hydrophilic domains. Such structural coherence in the hydrophilic segments is likely to positively influence ionic conductivity.

Mechanical/thermal properties

We assessed the mechanical properties of the membranes using an ultimate tensile strength machine (UTM). ***Figure 3c*** illustrates that membranes incorporating spirobifluorene as a branching agent exhibited enhanced tensile strength and elongation at break compared to membranes with varying amounts of spirobifluorene incorporation. Notably, the membrane designated as PBTPIPQ-SF2, which exhibited superior performance in ionic conductivity and SR, also achieved mechanical properties on par with those of PAP-TP-85, renowned for its exceptional toughness. Substitution of biphenyl with terphenyl in the membrane composition might result in a relatively less stiff backbone, which corresponded to a reduced maximum strength (PBTPIPQ-SF1: 45.06 MPa vs. PTPIPQ-SF1: 67.84 MPa). This alteration, however, led to an increase in elongation at break (PBTPIPQ-SF1: 20.2% vs. PTPIPQ-SF1: 9.1%), supporting a consistent trade-off between elongation at break and maximum strength, as noted in earlier studies.[33] Despite the reduced tensile strength, the enhancement in elongation at break allowed PBTPIPQ-SF1 to achieve a toughness about 1.7 times greater than PTPIPQ-SF1. PBTPIPQ-SF2 demonstrated higher tensile strength relative to PBTPIPQ-SF1. Contrary to earlier findings which suggested that an increase in crosslinking density typically boosts

maximum strength at the expense of elongation,[19, 34] PBTPIPQ-SF2 showed an increase in both parameters. This behavior parallels recent observations in 3D branched membranes enhanced with triptycene, where a higher molecular weight is expected to augment both maximum tensile strength and elongation at break.[20] Consequently, PBTPIPQ-SF2 exhibits approximately 1.6 times the toughness of PBTPIPQ-SF1. These robust mechanical properties are critical for the large-scale production of efficient hydrogen via membranes that meet rigorous mechanical standards.[33, 35] The enhanced durability of these membranes facilitates their use in membrane electrode assembly (MEA) processes, which operate at high temperatures above 100 ℃ and under significant current densities, ensuring stability and reduced cell resistance.[36]

Figure 3d presents the thermal gravimetric analysis (TGA) results of the prepared membranes. The analysis reveals that increasing the quantity of the crosslinking agent in the membranes (from PBTPIPQ-SF1 to PBTPIPQ-SF2) correlates with a rise in the temperature at which 5% weight loss ($T_{d5\%}$) occurs, climbing from 206.7 ℃ to 235 ℃. This enhancement in thermal stability facilitates reliable performance in the demanding conditions of high temperature and pressure, which are typical MEA processes and AEMWE applications.[37]

Alkaline stability test

A significant challenge in the long-term operation of AEM systems is the degradation caused by the attack of hydroxide ions on ion exchange groups, particularly in high-temperature environments. This degradation often leads to decreased ionic conductivity. To address this, the materials synthesized have been engineered to include stable ion exchange groups. Specifically, in the current study, piperidinium, a type of cyclic ammonium compound, was selected for its robustness in harsh conditions. Piperidinium demonstrates exceptional stability in a 1 M KOH solution at 80 ℃, owing to its unfavorable transition state for the primary degradation pathway, the Hoffman elimination, and a minimal S_N2 reaction.[9, 38] In a previous study, PTPIPQ, which possesses the stable ammonium moiety piperidinium and an aryl backbone of p-terphenyl without aryl ether structures, exhibited less than 5% degradation of its ion exchange groups after 360 h at 2 M NaOH, 90 °C.[38] Similarly, PFTP-13, constructed with p-terphenyl and fluorene, experienced less than 5% degradation after 1000 h at 1 M NaOH and 80 °C, and approximately 10% degradation at 5 M NaOH, 80 °C.[39] These results suggest that structures devoid of aryl ether motifs and featuring piperidinium as ammonium moieties demonstrate a heightened stability trend in alkaline environments. As depicted in ***Figure 3e***, based on the stable piperidinium structure and the absence of aryl ether motifs, PBTPIPQ-SF2 showed no signs of degradation after 1000 h of exposure to 1 M KOH at 80 °C, a finding confirmed by ^{1}H NMR analysis. Further analysis, as illustrated in ***Figure 3f*** and ***Figure S11***, reveals that under more extreme conditions—5 M KOH at 80 °C—PBTPIPQ-SF2 exhibited remarkable resistance to degradation, with only a 10.6% reduction in integrity after 500 h. This is attributed to the effects of hydroxide attack diminishing as the number of water

molecules around the hydroxide ion increases, which reduces the ion's nucleophilicity and basicity, thereby mitigating degradation.[40] Additionally, despite similar WU as PTPIPQ-SF1, PBTPIPQ-SF2 showed less degradation. The resilience observed could possibly be linked to the interconnected water channels within the membrane structure. These channels may effectively protect ion exchange groups from degradation by enhancing OH^- solvation, even under conditions of low water uptake.[41] Consequently, the high alkaline stability of PBTPIPQ-SF2 may be attributed by the stability of its aryl-based backbone, the strong stability of piperidinium as an ion exchange group, and the well-developed water channels within the membrane.

Cell test

Figure 4a describes the various components integral to an anion exchange membrane water electrolysis (AEMWE) system, including the membrane, ionomer, catalyst, gas diffusion layer (GDL), bipolar plate, and end plate. The membrane's ionic conductivity is pivotal, significantly impacting the current flow within the system and thereby influencing overall performance.[7, 42] Introducing a membrane like PBTPIPQ-SF2 with high ionic conductivity into the system can considerably enhance the current density achieved.[31a] The performance test of AEMWE utilized small amounts of catalysts, with IrO_2 (2.0 mg/cm^2) for the anode and PtRu/C (0.4 mg/cm^2) for the cathode. An ionomer—very recently developed by Lee et al. —was prepared by modifying a previously reported alkyl ammonium functionalized poly(carbazole) (QPC-TMA). To ensure a precise comparison of the membranes' performance, all other conditions were standardized, including the use of the same catalyst and ionomer components.[43]

Figures 4b and ***4c*** highlight how variations in ionic conductivity under identical operational conditions (excluding the membrane) can affect performance. Specifically, PBTPIPQ-SF2 shows ionic conductivity rates of approximately 161 mS/cm at 60 °C and 190 mS/cm at 80 °C. In comparison, the conductivity rates of commercial membranes like FAA-3 are 30 mS/cm and 60 mS/cm, respectively, illustrating more than a threefold increase in conductivity for PBTPIPQ-SF2. This substantial increase results in significant differences in current density, recording values of 6.17 A/cm^2 and 11.2 A/cm^2 at 60 °C and 80 °C for PBTPIPQ-SF2, versus 2.83 A/cm^2 and 4.25 A/cm^2 for FAA-3, respectively, thereby greatly enhancing hydrogen production rates.

Electrochemical impedance spectroscopy (EIS) analysis, as shown in ***Figures 4d*** and ***4e***, confirms that the higher ionic conductivity of PBTPIPQ-SF2 compared to FAA-3 leads to a marked reduction in both ohmic and system resistances, achieving an extremely low ohmic resistance of 0.025 Ω. This illustrates the critical role of membrane ionic conductivity in boosting cell performance. Moreover, ***Figure S12*** compares PBTPIPQ-SF2 with PTPIPQ-SF1, which shares the same composition except for the membrane. PBTPIPQ-SF2 exhibits about 1.6 times higher conductivity at 60 °C, enhancing cell performance to 6.17 A/cm^2 at 2 V

compared to 4.53 A/cm^2 for PTPIPQ-SF1. ***Figure S13*** shows that incorporating spirobifluorene as a 3D branching agent into the membrane not only boosts ionic conductivity but also achieves performance comparable to state-of-the-art systems with significantly less PGM catalyst used at the cathode and anode.

However, challenges remain in ionomer compatibility, as indicated in ***Table S2***. While PBTPIPQ-SF2 dissolves well in protic solvents such as DMSO, it exhibits poor solubility in more polar solvents, such as isopropanol (IPA) and deionized water (DI), commonly used in ink formulations. Even using the same ionomer, the choice of solvent can drastically impact performance due to potential agglomeration, leading to performance degradation.[44] Given the bulky, kinked structure of spirobifluorene, it is projected to enhance performance by increasing separation between the catalyst and phenyl groups and facilitating gas transport in structures with large free volume.[45] Future research is thus directed towards developing ionomers with high ion exchange capacities that dissolve effectively in solvents similar to those used in ink formulations, addressing these performance challenges.

CONCLUSIONS

In summary, we have developed high-performance membranes by introducing 9,9'-spirobifluorene as a 3D branching agent, effectively overcoming the conventional trade-off between ion conductivity and dimensional stability. Interestingly, the addition of this branching agent led to simultaneous improvements in both conductivity and dimensional stability. By adjusting the ratio of terphenyl to biphenyl and the amount of the branching agent, we optimized an AEM, specifically PBTPIPQ-SF2, which exhibits very high conductivity (190 mS/cm at 80 °C in 1 M KOH) along with decent WU, SR, and mechanical properties, comparable to the recently reported state-of-the-art membrane. Through gas pycnometry and AFM investigations, we discovered that spirobifluorene increases the fractional free volume around the backbone and enhances the phase separation between the hydrophobic and hydrophilic domains more delicately, thereby boosting ion conductivity and mechanical/dimensional stability. PBTPIPQ-SF2 also demonstrated excellent chemical stability, showing no observable degradation at 80 °C in 1 M KOH over 1000 h and only 10.56 % degradation at 80 °C in 5 M KOH over 500 h. With such membranes, an excellent current density of 11.2 A/cm^2 was achieved with low catalyst loading, attributed to the low ohmic resistance. We believe this technology is crucial for the future commercialization of AEMWEs, surpassing both the ionic conductivity and current density of cation exchange membranes. Furthermore, we anticipate that the bulky structure of spirobifluorene can address issues such as phenyl adsorption by facilitating its dissolution in ink solvents, thus enhancing performance.

ACKNOWLEDGMENTS

This work was supported by the KRISS (Korea Research Institute of Standards and Science) MPI Lab. program. The work from KRICT was supported by the Korea Institute of Energy Technology Evaluation and Planning (KETEP) grant (20203020030010) funded by the Ministry of Trade, Industry & Energy (MOTIE, Korea)

COMPETING INTERESTS

Patent application (K.R. application number: 10-2023-0165585) filed by G. W. R., G. C. K., S. H. P., and M.S.K. from KRISS.

REFERENCES

[1] N. Du, C. Roy, R. Peach, M. Turnbull, S. Thiele, C. Bock, *Chem. Rev.* **2022**, 122, 11830.

[2] Y. Yang, P. Li, X. Zheng, W. Sun, S. X. Dou, T. Ma, H. Pan, *Chem. Soc. Rev.* **2022**, 51, 9620.

[3] N. Chen, Y. M. Lee, *Prog. Polym. Sci.* **2021**, 113, 101345

[4] Z. Sun, B. Lin, F. Yan, *ChemSusChem* **2018**, 11, 58.

[5] X. Ge, F. Zhang, L. Wu, Z. Yang, T. Xu, *Macromolecules* **2022**, 55, 3773.

[6] J. Xue, J. Zhang, X. Liu, T. Huang, H. Jiang, Y. Yin, Y. Qin, M. D. Guiver, *Electrochem. Energ. Rev.* **2021**, 5, 348.

[7] W. E. Mustain, M. Chatenet, M. Page, Y. S. Kim, *Energy Environ. Sci.* **2020**, 13, 2805.

[8] a) Y.-K. Choe, C. Fujimoto, K.-S. Lee, L. T. Dalton, K. Ayers, N. J. Henson, Y. S. Kim, *Chem. Mater.* **2014**, 26, 5675; b) A. D. Mohanty, S. E. Tignor, J. A. Krause, Y.-K. Choe, C. Bae, *Macromolecules* **2016**, 49, 3361.

[9] M. G. Marino, K. D. Kreuer, *ChemSusChem* **2015**, 8, 513.

[10] a) B. Lin, F. Chu, Y. Ren, B. Jia, N. Yuan, H. Shang, T. Feng, Y. Zhu, J. Ding, *J. Power Sources* **2014**, 266, 186; b) Z. Sun, J. Pan, J. Guo, F. Yan, *Adv. Sci.* **2018**, 5, 1800065.

[11] G. W. Ryoo, S. H. Park, K. C. Kwon, J. H. Kang, H. W. Jang, M. S. Kwon, *J. Energy Chem.* **2024**, 93, 478

[12] H. Chen, R. Tao, K. T. Bang, M. Shao, Y. Kim, *Adv. Energy Mater.* **2022**, 12, 2200934

[13] N. Chen, C. Hu, H. H. Wang, S. P. Kim, H. M. Kim, W. H. Lee, J. Y. Bae, J. H. Park, Y. M. Lee, *Angew, Chem. Int. Ed.* **2021**, 60, 7710.

[14] S. Noh, J. Y. Jeon, S. Adhikari, Y. S. Kim, C. Bae, *Acc. Chem. Res.* **2019**, 52, 2745.

[15] a) J. Ran, L. Wu, Y. He, Z. Yang, Y. Wang, C. Jiang, L. Ge, E. Bakangura, T. Xu, *J. Memb. Sci.* **2017**,

522, 267; b) Y. Ma, C. Hu, G. Yi, Z. Jiang, X. Su, Q. Liu, J. Y. Lee, S. Y. Lee, Y. M. Lee, Q. Zhang, *Angew, Chem. Int. Ed.* **2023**, 135, e202311509.

[16] J. Wang, Y. Zhao, B. P. Setzler, S. Rojas-Carbonell, C. Ben Yehuda, A. Amel, M. Page, L. Wang, K. Hu, L. Shi, S. Gottesfeld, B. Xu, Y. Yan, *Nat. Energy* **2019**, 4, 392.

[17] L. Bai, L. Ma, L. Li, A. Zhang, X. Yan, F. Zhang, G. He, *ACS Appl. Energy Mater.* **2021**, 4, 6957.

[18] X. Wu, N. Chen, H. A. Klok, Y. M. Lee, X. Hu, *Angew, Chem. Int. Ed.* **2022**, 61, e202114892.

[19] Q. Liu, S. Zhang, L. Tian, J. Li, W. Ma, F. Wang, Z. Wang, J. Li, H. Zhu, *J. Power Sources* **2023**, 564, 232822.

[20] C. Hu, N. Y. Kang, H. W. Kang, J. Y. Lee, X. Zhang, Y. J. Lee, S. W. Jung, J. H. Park, M.-G. Kim, S. J. Yoo, S. Y. Lee, C. H. Park, Y. M. Lee, *Angew, Chem. Int. Ed.* **2024**, 63, e202316697.

[21] C. Chen, X. Zeng, Z. Peng, Z. Chen, *J. Appl. Polym. Sci.* **2023**, 140, e53795.

[22] a) M. T. Guzmán-Gutiérrez, D. R. Nieto, S. Fomine, S. L. Morales, M. G. Zolotukhin, M. C. G. Hernandez, H. Kricheldorf, E. S. Wilks, *Macromolecules* **2010**, 44, 194; b) H. Gao, *ACS Omega* **2021**, 6, 4527.

[23] G. Xu, J. Pan, X. Zou, Z. Jin, J. Zhang, P. Fang, Q. Zhang, Z. Sun, F. Yan, *Adv. Func. Mater.* **2023**, 33, 2302364.

[24] F. Xu, Y. Li, J. Ding, B. Lin, *ChemElectroChem* **2023**, 10, e202300445.

[25] X. Wang, C. Lin, Y. Gao, R. G. Lammertink, *J. Memb. Sci.* **2021**, 635, 119525.

[26] X. Wu, N. Chen, C. Hu, H. A. Klok, Y. M. Lee, X. Hu, *Adv. Mater.* **2023**, 35, e2210432.

[27] S. Zhang, X. Li, Y. Yang, J. Li, J. Zheng, S. Zhang, *J. Memb. Sci.* **2024**, 122587.

[28] a) C. Chen, Y. L. Tse, G. E. Lindberg, C. Knight, G. A. Voth, *J. Am. Chem. Soc.* **2016**, 138, 991; b) L. Ma, M. Hussain, L. Li, N. A. Qaisrani, L. Bai, Y. Jia, X. Yan, F. Zhang, G. He, *J. Memb. Sci.* **2021**, 636; c) S. C. Ramírez, R. R. Paz, *New Trends in Ion Exchange Studies* **2018**, 51.

[29] W. T. Gao, X. L. Gao, W. W. Gou, J. J. Wang, Z. H. Cai, Q. G. Zhang, A. M. Zhu, Q. L. Liu, *J. Memb. Sci.* **2022**, 655, 120578.

[30] S. Miyanishi, T. Yamaguchi, *J. Mater. Chem. A* **2019**, 7, 2219.

[31] a) C. Hu, H. W. Kang, S. W. Jung, M. L. Liu, Y. J. Lee, J. H. Park, N. Y. Kang, M. G. Kim, S. J. Yoo, C. H. Park, *Adv. Sci.* **2024**, 2306988; b) Y. Kim, Y. Wang, A. France-Lanord, Y. Wang, Y. M. Wu, S. Lin, Y. Li, J. C. Grossman, T. M. Swager, *J. Am. Chem. Soc.* **2019**, 141, 18152.

[32] J. Zhang, K. Zhang, X. Liang, W. Yu, X. Ge, M. A. Shehzad, Z. Ge, Z. Yang, L. Wu, T. Xu, *J. Mater. Chem. A* **2021**, 9, 327.

[33] M. Liu, X. Hu, B. Hu, L. Liu, N. Li, *J. Memb. Sci.* **2022**, 642, 119966.

[34] M. S. Cha, J. Y. Lee, T.-H. Kim, H. Y. Jeong, H. Y. Shin, S.-G. Oh, Y. T. Hong, *J. Memb. Sci.* **2017**, 530, 73.

[35] W. Song, K. Peng, W. Xu, X. Liu, H. Zhang, X. Liang, B. Ye, H. Zhang, Z. Yang, L. Wu, X. Ge, T. Xu,

Nat Commun **2023**, 14, 2732.

[36] G. Sriram, K. Dhanabalan, K. V. Ajeya, K. Aruchamy, Y. C. Ching, T. H. Oh, H.-Y. Jung, M. Kurkuri, *J. Mater. Chem. A* **2023**, 11, 20886.

[37] Q. Xu, L. Zhang, J. Zhang, J. Wang, Y. Hu, H. Jiang, C. Li, *EnergyChem* **2022**, 4, 100087.

[38] J. S. Olsson, T. H. Pham, P. Jannasch, *Adv. Func. Mater.* **2017**, 28, 1702758.

[39] N. Chen, H. H. Wang, S. P. Kim, H. M. Kim, W. H. Lee, C. Hu, J. Y. Bae, E. S. Sim, Y. C. Chung, J. H. Jang, S. J. Yoo, Y. Zhuang, Y. M. Lee, *Nat Commun* **2021**, 12, 2367.

[40] a) L. Liu, L. Bai, Z. Liu, S. Miao, J. Pan, L. Shen, Y. Shi, N. Li, *J. Memb. Sci.* **2023**, 665, 121135; b) D. R. Dekel, M. Amar, S. Willdorf, M. Kosa, S. Dhara, C. E. Diesendruck, *Chem. Mater.* **2017**, 29, 4425; c) D. R. Dekel, S. Willdorf, U. Ash, M. Amar, S. Pusara, S. Dhara, S. Srebnik, C. E. Diesendruck, *J. Power Sources* **2018**, 375, 351; d) S. Willdorf-Cohen, A. N. Mondal, D. R. Dekel, C. E. Diesendruck, *J. Mater. Chem. A* **2018**, 6, 22234.

[41] a) F. Xu, Y. Su, B. Lin, *Front. Mater.* **2020**, 7:4; b) L. Zhu, X. Peng, S. L. Shang, M. T. Kwasny, T. J. Zimudzi, X. Yu, N. Saikia, J. Pan, Z. K. Liu, G. N. Tew, W. E. Mustain, M. Yandrasits, M. A. Hickner, *Adv. Func. Mater.* **2019**, 29, 1902059; c) K. Zhang, W. Yu, X. Ge, L. Wu, T. Xu, *J. Memb. Sci.* **2022**, 661, 120922; d) X. Du, H. Zhang, Y. Yuan, Z. Wang, *J. Power Sources* **2021**, 487, 229429.

[42] a) S. Y. Kang, J. E. Park, G. Y. Jang, O.-H. Kim, O. J. Kwon, Y.-H. Cho, Y.-E. Sung, *Int. J. Hydrogen Energy* **2022**, 47, 9115; b) S. A. Lee, J. Kim, K. C. Kwon, S. H. Park, H. W. Jang, *Carbon Neutralization* **2022**, 1, 26.

[43] M. S. Cha, J. E. Park, S. Kim, S.-H. Han, S.-H. Shin, S. H. Yang, T.-H. Kim, D. M. Yu, S. So, Y. T. Hong, S. J. Yoon, S.-G. Oh, S. Y. Kang, O.-H. Kim, H. S. Park, B. Bae, Y.-E. Sung, Y.-H. Cho, J. Y. Lee, *Energy Environ. Sci.* **2020**, 13, 3633.

[44] E. Cossar, F. Murphy, J. Walia, A. Weck, E. A. Baranova, *ACS Appl. Energy Mater.* **2022**, 5, 9938.

[45] X. Luo, D. I. Kushner, J. Li, E. J. Park, Y. S. Kim, A. Kusoglu, *Adv. Func. Mater.* **2021**, 31, 2008778.

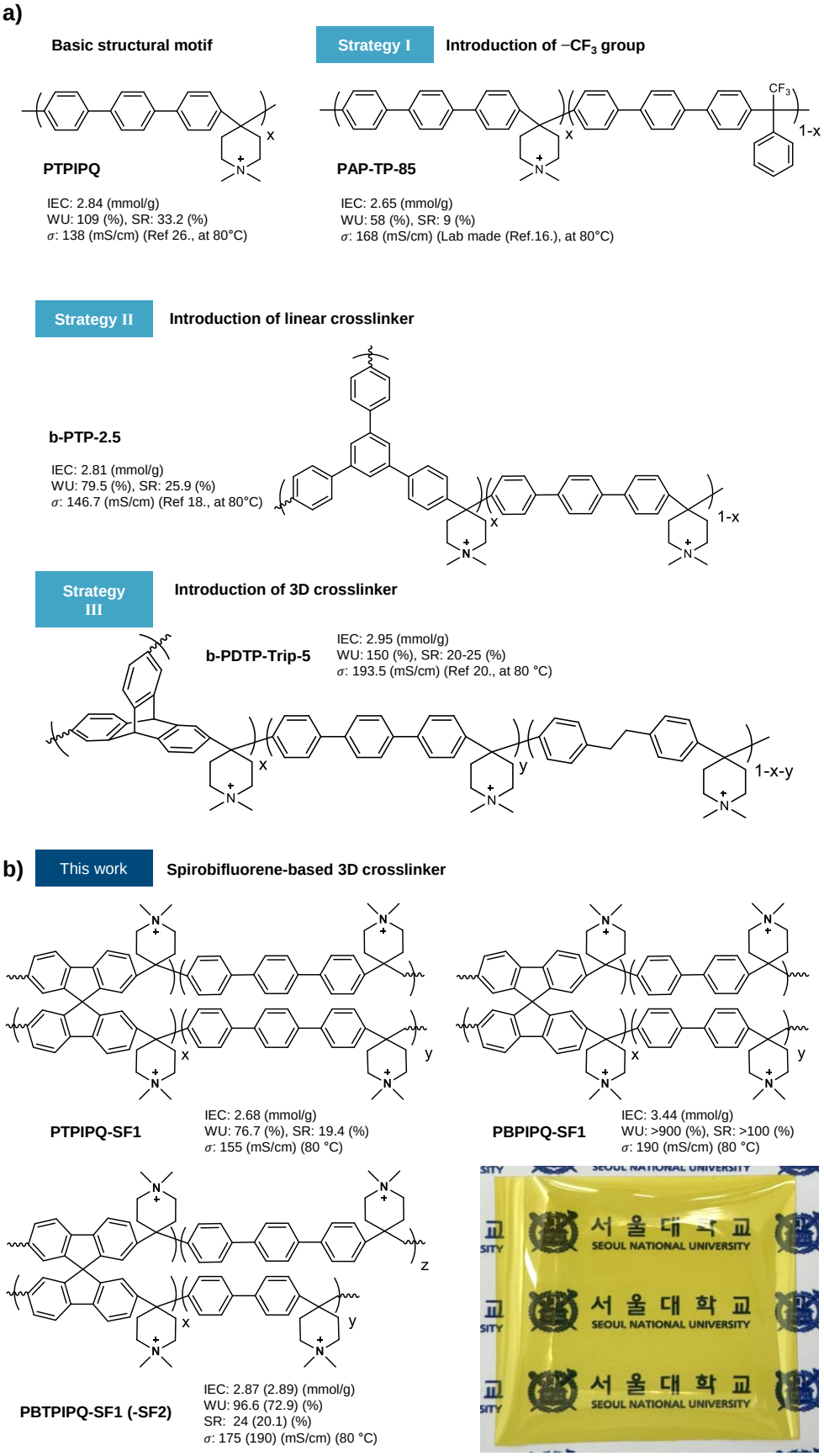

Figure 1. Structures of AEMs (a) Past research strategies employed for enhancing properties of membranes (b) Strategy of introducing spirobifluorene as a 3D crosslinker

Table 1. Various physical properties of PTPIPQ-SF1, PBPIPQ-SF1, PBTPIPQ-SF1, PBTPIPQ-SF2 and reference membranes

AEMs		*IEC (mmol/g)* [a]		*WU (%)* [a]		*SR (%)* [a]		*σ (mS/cm)* [b]		*λ*	
		Theor	*Titration*	*40 ℃*	*80 ℃*	*40 ℃*	*80 ℃*	*40 ℃*	*80 ℃*	*40 ℃*	*80 ℃*
PTPIPQ-SF1		2.8	2.7	51.2	76.7	8.6	19.4	93	155	10.6	15.9
PBPIPQ-SF1		3.5	3.4	> 900	> 900	> 100	> 100	123	190	> 100	> 100
PBTPIPQ-SF1		2.9	2.9	64.7	96.6	8.9	24.0	115	175	12.5	18.7
PBTPIPQ-SF2		2.9	2.9	55.6	79.6	8.1	20.1	120	190	10.7	14
Reference	PTPIPQ (PAP)	2.8	2.8 [c]	94	109	30.7	33.2	81	138	-	-
	PAP-TP-85 (PiperION, lab made)	2.8	2.7 [d]	34.3	56.2	6.4	11.8	84	151	6.9	11.3
		2.4[e, f]	2.4[e, f]	~50	~55	~7.5	~10	~100	~170	-	-
	FAA-3 (Fumatech)	-	2.1[g]	75.1	153.8	14.5	37.5	25	60	19.8	40.7
		-	2.1[h]	~60	~90	~20	~30	~40	~80	~15	~23

[a] Correspond to the values in the OH^- form. [b] 1 M KOH condition [c] Data of ref. 26 [d] Measurements were conducted using a lab made membrane according to ref. 16 [e] I^- form [f] Data of ref. 16 [g] Measurements were conducted using commercially available membranes [h] Data of ref. 25

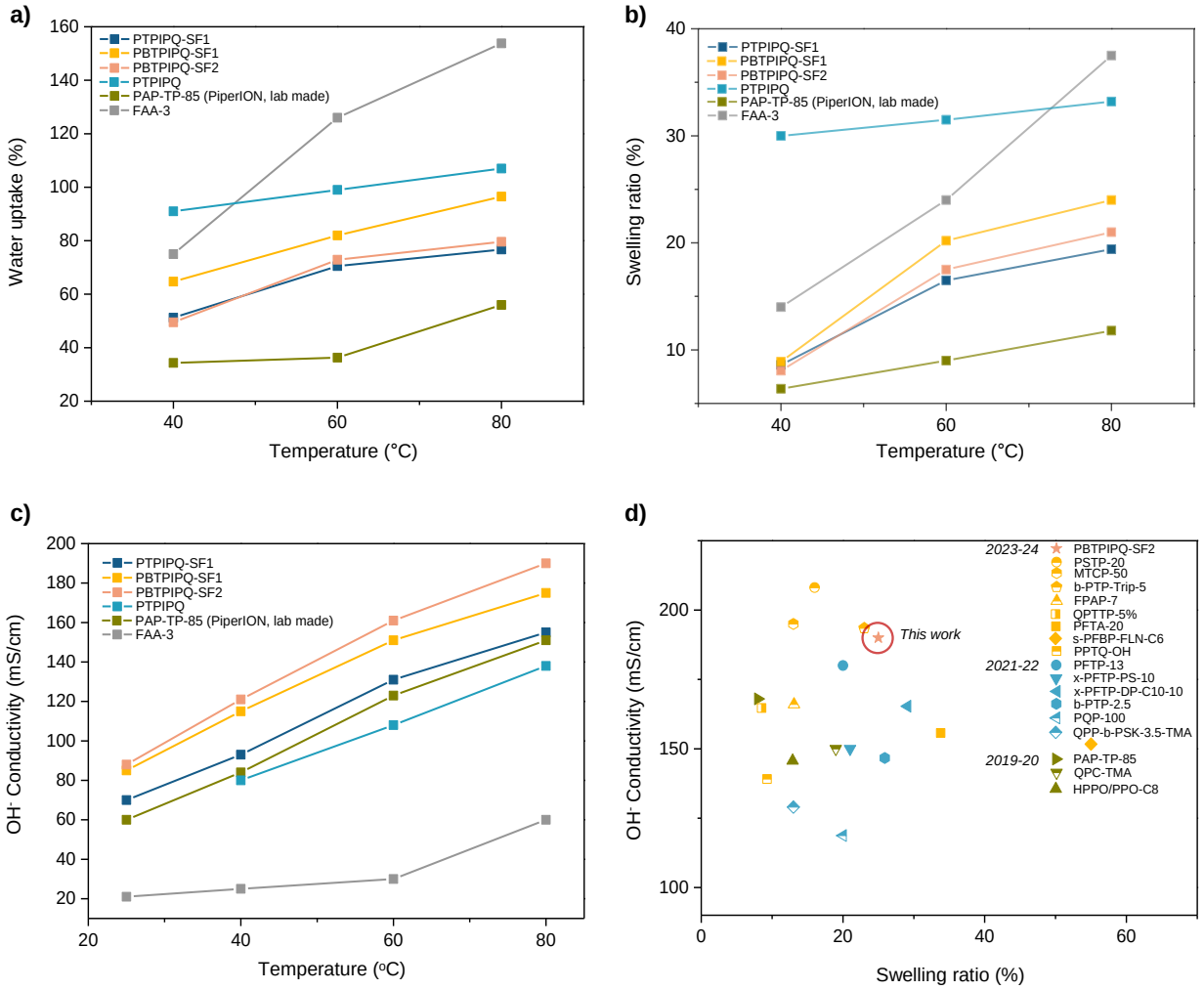

Figure 2. Differernce of properties between –SF1 or –SF2 membranes and reference membranes (PTPIPQ, PAP-TP-85 and FAA-3) (a) Water uptake (WU) (b) Swelling ratio (SR) (c) OH^- conductivity of AEMs at different temperatures (100% RH) (d) Comparison of the OH^- conductivity between PBTPIPQ-SF2 in this work and state-of-the-arts in previous work

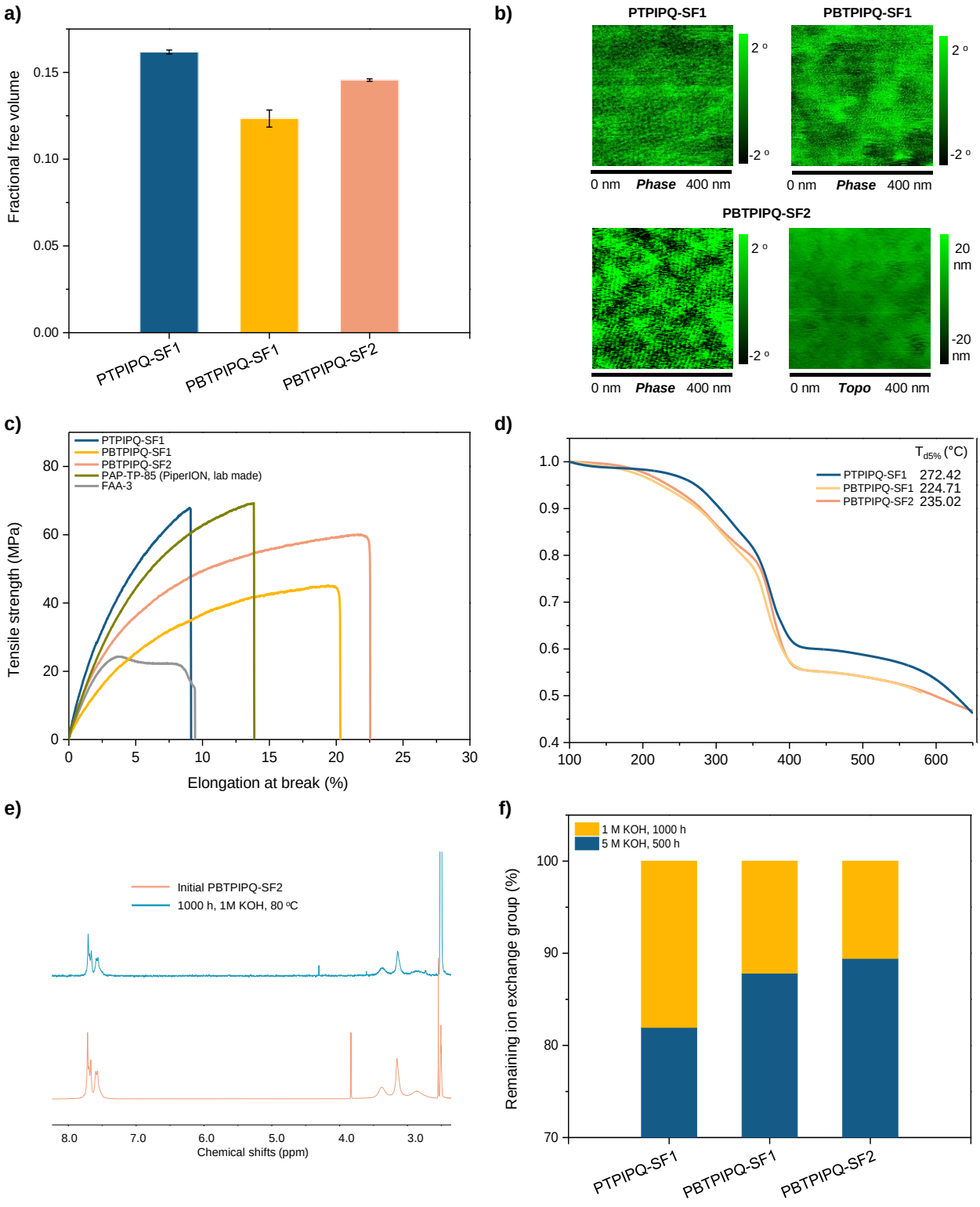

Figure 3. (a) Fractional free volume of PTPIPQ-SF1, PBTPIPQ-SF1 and PBTPIPQ-SF2 (b) AFM phase images of PTPIPQ-SF1, PBTPIPQ-SF1, PBTPIPQ-SF2 and topography image of PBTPIPQ-SF2 (c) Mechanical properties of PTPIPQ-SF1, PBTPIPQ-SF1, PBTPIPQ-SF2 and reference AEM (PAP-TP-85, FAA-3) (d) Thermal properties of PTPIPQ-SF1, PBTPIPQ-SF1 and PBTPIPQ-SF2 (e) Alkaline stability of PBTPIPQ-SF2 in 1 M KOH at 80 °C (f) Remaining ion exchange group of PTPIPQ-SF1, PBTPIPQ-SF1 and PBTPIPQ-SF2 in 1 M KOH, 5 M KOH at 80 °C

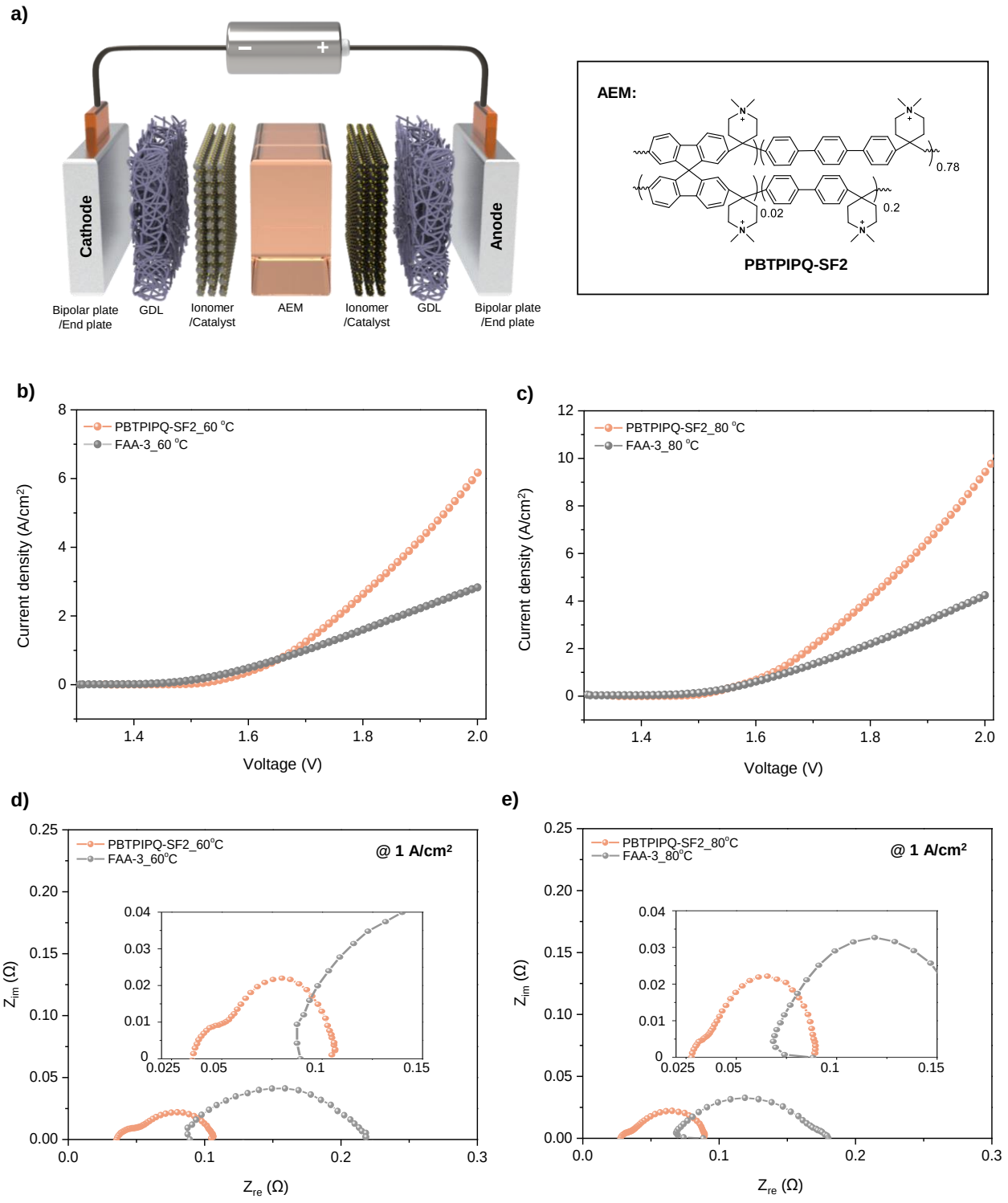

Figure 4. (a) Illustration of anion exchange membrane and ionomer in AEMWEs (b) I-V polarization curves spectra of PBTPIPQ-SF2 and commercial membrane (FAA-3) at 60 °C (c) I-V polarization curves spectra of PBTPIPQ-SF2 and commercial membrane (FAA-3) at 80 °C (d) EIS analysis of PBTPIPQ-SF2 and commercial membrane at 60 °C for the AEMWE (e) EIS analysis of PBTPIPQ-SF2 and commercial membrane at 80 °C for the AEMWEs